Using an AUV to Measure Wavelength Attenuation of Sunlight in Water

Max Conine
Harvey Mudd College
Claremont, CA
mconine@g.hmc.edu

***Abstract*—The goal of our project was to measure how light wavelength relative intensities vary with depth underwater. Measuring the temperature of and how light travels through a volume of water can tell us how clean a column of water is and also help us understand the composition of that water [1], [2], [3]. To achieve this goal, we built an Autonomous Underwater Vehicle (AUV) that can dive over 5 meters underwater and measure 12 channels of light wavelengths at varying depths. We used a spectral sensor to measure the wavelengths of light underwater, a thermistor to measure water temperature, and a GoPro to normalize our spectral data. Our data generally showed that longer wavelengths, particularly 745 nm and 855 nm, attenuated more rapidly than shorter wavelengths as expected (Fig. 14). Our thermistor sensor failed to produce meaningful results of water temperature of water at depth, however it provided us with water temperature at the surface. The pressure sensor produced reliable depth measurements throughout all trials.**

I. Introduction

Light traveling through water is attenuated due to absorption and scattering depending on the light wavelength, with shorter wavelengths penetrating deeper in water than longer wavelengths [1]. The light entering water will not change frequency but will change intensity [1]. This phenomenon can be described by the Bouguer-Beer-Lambert law, which states that the intensity of light decreases exponentially as it passes through a medium [4]. The fundamental equation describing exponential attenuation of light intensity is given by the Beer–Lambert law:

$$A(\lambda) = -\log_{10}\left(\frac{I(\lambda)}{I_0(\lambda)}\right) = \varepsilon(\lambda)\cdot c\cdot l \qquad (1)$$

Where $A(\lambda)$ is the absorbance, which measures the amount of light at a specific wavelength λ that is attenuated. $I_0(\lambda)$ is the initial intensity of light at wavelength λ before entering the sample, $I(\lambda)$ is the intensity of light at wavelength λ. $\varepsilon(\lambda)$ is the molar attenuation coefficient, which represents how strongly a volume attenuates light at a given wavelength. c is the concentration of the attenuating species in the medium, and l is the path length that the light travels through the material. Thus, in (1) we see that the ratio of transmitted intensity to incident intensity $\frac{I}{I_0}$ is related to properties of the medium through a negative logarithm.

We can see absorption and scattering illustrated in Fig. 1 where it's clear that composition of the water affects attenuation. The wavelengths that are attenuated quicker in more shallow depths depend on the composition of the water [5].

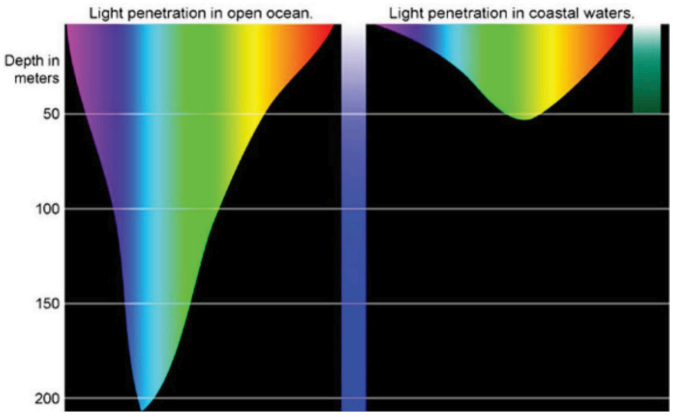

Fig. 1. Basic illustration of how different colors of light penetrate ocean waters courtesy of NOAA Ocean Exploration [5].

This wavelength-dependent attenuation is important for understanding underwater visibility and optical sensing. Water temperature can also affect water clarity as warmer water temperatures can increase growth of algae and phytoplankton which can make the water more murky [3].

In this project, we aim to explore this phenomenon by taking real measurements of how light intensity changes with depth using an AUV equipped with a spectral sensor that senses 12 channels of wavelengths ranging from about 405 to 855 nm [6], a thermistor sensor to measure water temperature, and a pressure sensor to measure depth of the AUV. By collecting spectral data at different depths, we aim to discover how different wavelengths attenuate in a real marine environment and compare those trends to expected behavior. This real data can be used to estimate the clarity and composition of water

when compared with theoretical and baseline data and to help scientists study water quality and composition.

II. Sensor Design

In order to measure how light attenuation is affected by depth under the surface, we need to measure AUV depth and light wavelength relative intensities. In addition, we can measure water temperature to help better understand water conditions as temperature can affect the clarity and composition of sea water [2]. We selected sensors that fit within a $50 budget, while maximizing the robustness and accuracy of our sensors.

We chose the MPX5700ASX-ND pressure sensor as the analog output allowed us to tune the sensor range and accuracy, as well as the sensor was available in the E80 lab and we had previous experience using it [7]. The MPX5700ASX-ND measures pressure and produces voltage corresponding to pressure linearly according to equation (2).

$$V_{\text{out}} = V_{\text{supply}(0.0012858 \cdot P + 0.04)} \tag{2}$$

At 0 to 5 meters of depth, the output ranges from 0.851 to 1.175 volts [7]. To improve the accuracy of our readings, we used an offset amplifier circuit (Fig. 2) to shift the range of output voltages to 0.21 to 2.9 V at respective 0 meter and 5 meter depths. Since the input range of our Teensy microcontroller is 0 to 3.3 V, the circuit output voltage leaves room for the AUV to dive deeper than 5 meters without clipping.

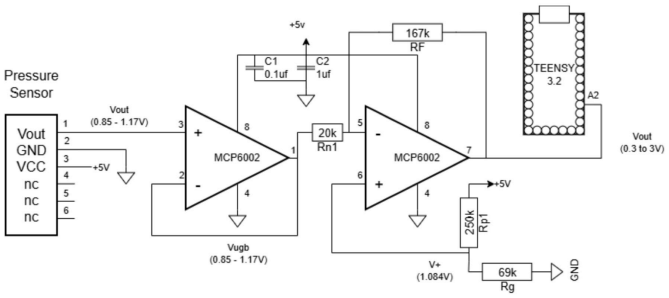

Fig. 2. Pressure Sensor Circuit.

As shown in Fig. 2, we provide a unity gain buffer on the output of the pressure sensor and then use an offset amplifier circuit to fit the voltages into the desired range. We used 2 MCP6002 op-amps to accomplish this. The offset amplifier obeys the following equation (3), where V_{out} is the circuit output voltage, V_+ is the input voltage.

$$\left(1 + \frac{R_f}{R_{\text{n1}}}\right) V_+ - \frac{R_f}{R_{\text{n1}}} = V_{\text{out}} \tag{3}$$

We chose R_{n1} as 20 kΩ and R_f as 167 kΩ as shown in Fig. 2. We calibrated our sensor by taking voltage measurements on our teensy at varying known depths and finding the relationship between voltage and depth to make a line of best fit (Fig. 3). Software was added to interpret the pressure sensor readings and convert sensor voltage into depth.

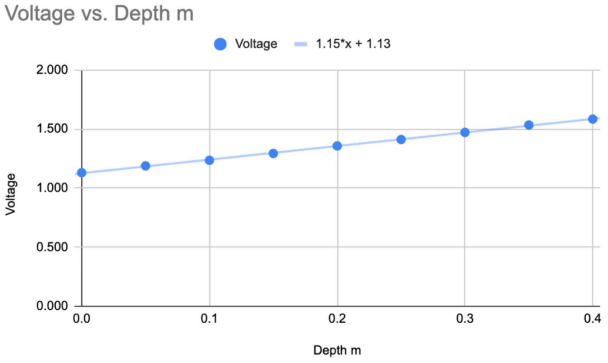

Fig. 3. Pressure sensor calibration curve.

For measuring temperature, we chose to use the 490-5633-ND 100 kΩ thermistor [8] in order to maximize robustness and reliability of the sensor while minimizing our cost. This sensor was available in the E80 lab, which made it an obvious choice. The high nominal resistance makes it resist self-heating which can skew readings [8]. It's also a negative temperature coefficient thermistor, so it drops resistance as it increases in temperature and is able to measure temperature with extreme sensitivity [8]. In addition it has a fast response time which makes it a great choice for our application. We used a voltage divider and offset amplifier circuit shown in Fig. 4 to convert resistance into a readable voltage that our Teensy can log.

We expect the water temperature at Dana Point to be within 5 to 22.5 °C. We designed our circuit to give us an output voltage ranging from 1.32 V to 2.34 V at the ends of this range.

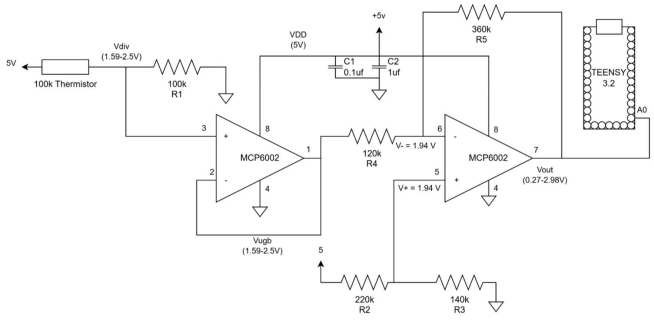

Fig. 4. Thermistor Interface Circuit.

We added software to interpret the voltage using a linear fit and estimate the water temperature. To calibrate our sensor, we measured a range of water temperatures

and corresponding voltages and approximated a line of best fit as shown in Fig. 5.

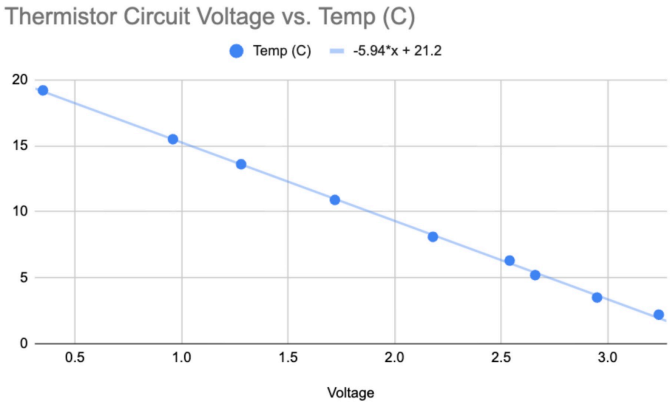

Fig. 5. Thermistor Calibration Curve.

For measuring intensities of light across a spectrum of wavelengths, we chose the AS7343_Qwiic spectral sensor [6] as it best fit our objectives to maximize reliability and minimize cost. The AS7343_Qwiic spectral sensor was also chosen because it gave us lots of information about the relative intensities of numerous wavelengths, which was what we wanted to analyze. The AS7343_Qwiic sensor is able to output relative intensities of light wavelengths on a scale ranging from 0 to 1000 of 12 channels of different wavelengths ranging from 405 nm to 855 nm. [6]

We designed a circuit as shown in Fig. 6 to connect the sensor to our teensy using the I2C digital interface. Our teensy has two dedicated pins for I2C interfaces on pins 18 and 19. To connect to the sensor, we used code provided by the manufacturer modified to collect and log data of each channel of the sensor during a dive [6].

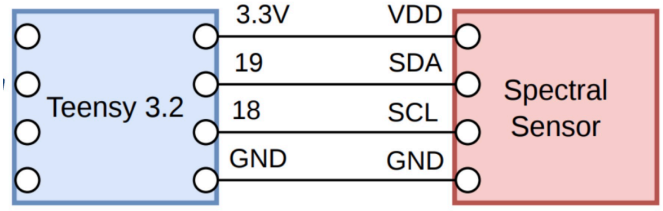

Fig. 6. Spectral Sensor Interface Circuit.

The software modifications include turning off the light during deployment and writing code to log data on each channel every loop.

We validated our sensor by testing it in the lab against known colors to make sure it was reading wavelengths correctly and quickly. We also made sure that the light intensity was working by covering the sensor slowly and watching the relative intensities of all wavelengths lower to 0.

III. Robot Design

Our AUV was designed with the constraints of being able to dive over 5 meters and have a location on the top of the AUV to mount the spectral sensor to. We designed the robot with the goal of maximizing simplicity and robustness. The overall archetype consists of a 3 motor, neutrally buoyant, roughly 7″ x 8″ x 5.5″ diving robot (Fig. 8). We avoided using pool noodles because they compress under high pressure and affect AUV buoyancy.

We calculated the robot center of mass by summing up the pvc mass and motor mass at each location on the robot in 2 planes and dividing by total mass to get the X, Y, and Z coordinates of the center of mass (Fig. 7). We found the center of mass to be toward the front motor just under the center of the box, however, these positions changed when we went to deploy our robot since we adjusted battery position to make the robot float level.

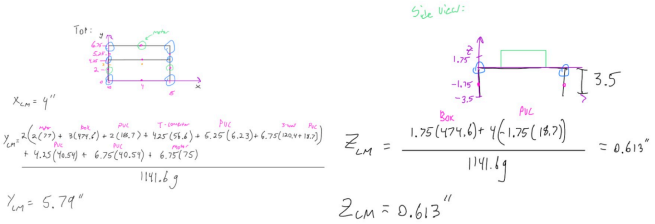

Fig. 7. X and Y and Z Center of Mass Calculations.

We used the center of mass calculation to determine where to place the box and where to place the battery in the box in order to make the robot sit level during its dive.

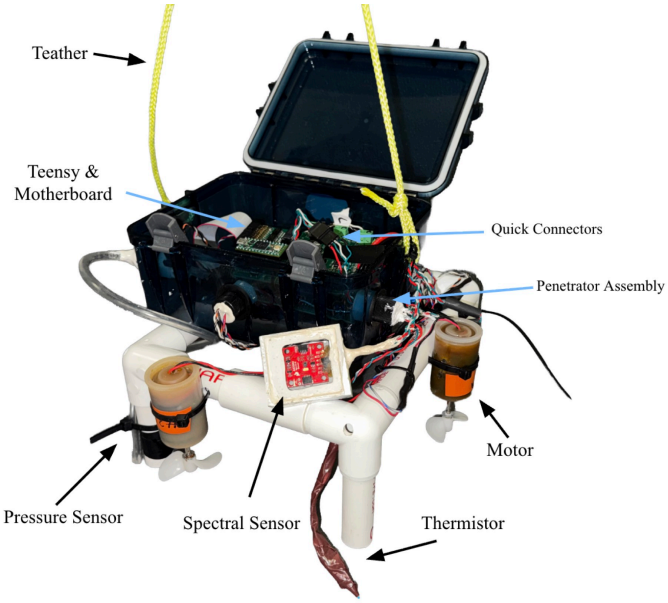

Fig. 8. Final AUV with components and sensors labeled.

As shown in Fig. 8, we designed our robot to be compact. We placed our spectral and GoPro sensors facing up to view the light coming from the surface. The spectral sensor housing box was designed to keep our sensor waterproof and not interfere with the wavelengths of light detected. We designed the housing out of billet aluminum with a quartz glass top, custom cut to fit the box. The aluminum was chosen to make the box water resistant at high depth and the quartz was chosen to not interfere with the wavelengths of light detected. Quartz glass (SiO_2) allows over 98% of visible light, UV, and infrared light to pass through without being obstructed due to its wide band gap and exceptional transparency [9]. We machined the housing out of aluminum billet according to the dimensions in Fig. 10.



Fig. 9. Photos showing spectral sensor housing before and after epoxying the SiO_2 quartz glass panel on.

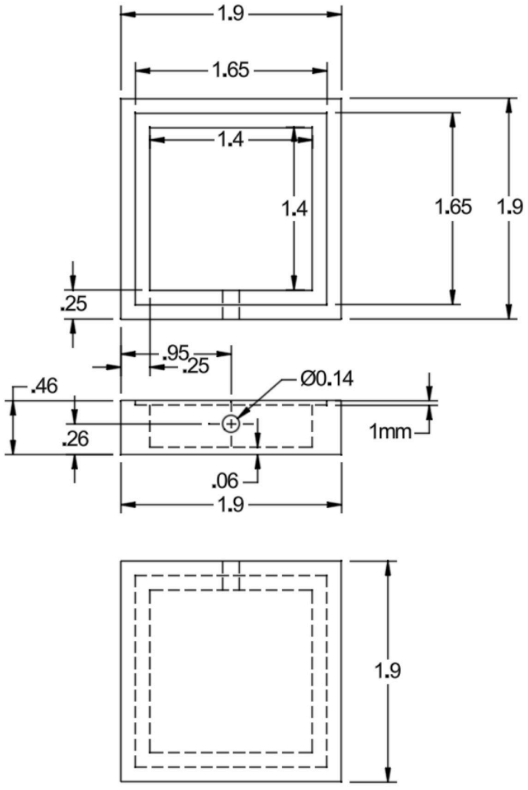

Fig. 10. Spectral sensor housing drawing.

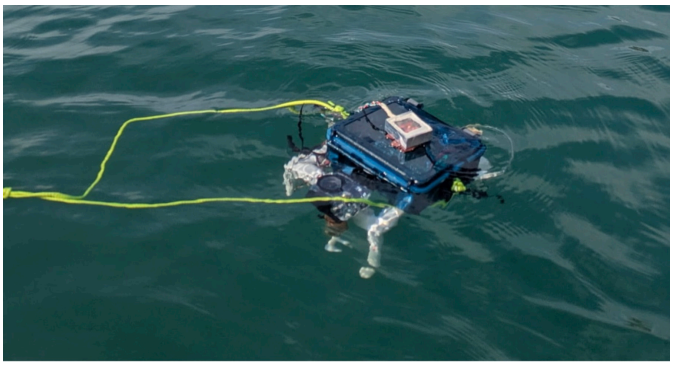

Fig. 11. Robot at the start of its deployment. Spectral sensor is clearly visible mounted on the top of the robot.

The robot software builds of the template code given by the E80 teaching team, modified to log data from each of the robot's sensors as well as print out the status of each sensor and detect if a sensor rails out. The loop frequency is 10 Hz and data is collected from each sensor offset sequentially throughout each loop.

IV. Deployment Details

Throughout the project, we deployed the robot over 20 times. Initial testing occurred in the tank room to ensure the robot was waterproof, then in Pitzer pool to get initial spectral sensor measurements, our first 3 meter dive occurred in Phake Lake, and the final deployments occurred at Dana Point. We found that 0.25 meter step increments with 7 seconds to sample at each step was the most effective way to make sure that robot had ample time to sample at each step with its motors off. We modified the code so once the robot reached its desired checkpoint, it turned off the motors while in the ± 0.2 meter range. The reason we turned the motors off is to reduce noise in our circuit measurements, as we found in previous trials that if the motors were on it disrupted how accurately the Teensy measured the sensor signals. We decided 5 meters was deep enough for us to measure how light change across a spectrum. We deployed across various times ranging from 9 am to 12pm in order to collect the most data with different amounts of initial sunlight. Throughout each deployment at Dana Point we followed the following testing protocol:

1) Paddle to deployment area shown in Fig. 12
2) Turn GoPro on and press record
3) Turn robot on
4) Close box carefully, making sure no wires are on seal that could cause a leakage
5) Position robot underwater so spectral sensor sits upright, tilt to remove air bubbles and test ballasting

6) Wait until motors run, then let go of the robot and position the kayak to not block natural sunlight sensed by the robot
7) Wait until robot resurfaces to pull robot back onto kayak using the tether
8) Turn robot off
9) Turn GoPro off

To ensure safety, we wore life jackets during deployments when in the kayaks or rowboat, dried the robot off before opening waterproof box to avoid water on electronics, charged the robot battery in a flame retardant case, and designed the robot with no sharp points that a user could cut themselves on. Additionally, we tethered our robot to the kayak during deployment to minimize risk of losing the robot. We made sure to not pollute the environment by ensuring the robot did not leave any components or residue behind.

We chose a deployment area that had over 5 meters of depth and had a clear view of the sun (Fig. 12). The depth charts of Dana Point were found on a public ocean depth mapping website [10]. The robot was programmed with a 30 second delay from when we turned it on to the time it started its motors, which allowed us time to seal the box up and place the robot in the water. After a successful trial, we pulled the log file off the onboard sd card on the robot and plotted the data using MATLAB. We did over 6 trials following the deployment procedure at Dana Point in order to better understand the uncertainty in our measurements needed to make conclusions.

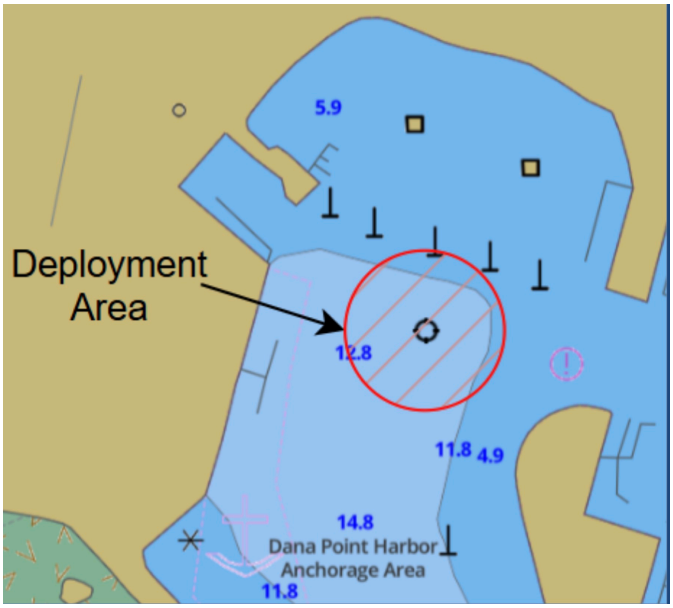

Fig. 12. Deployment area circled in red.



Fig. 13. Max switching robot on during deployment. Paddle boards were borrowed from a team member. Robot is shown tethered to the board.

V. Results

We found through throughout numerous trials the 745 nm wavelength was attenuated the most. We can model the light attenuation using the constants found by Pope & Fry in 1997 of attenuation constants over multiple wavelengths for pure water [11]. This is modeled in Fig. 14, with a comparison to our data collected on the left. We see in Fig. 14 there is a general trend of decrease in light intensity as depth increases.

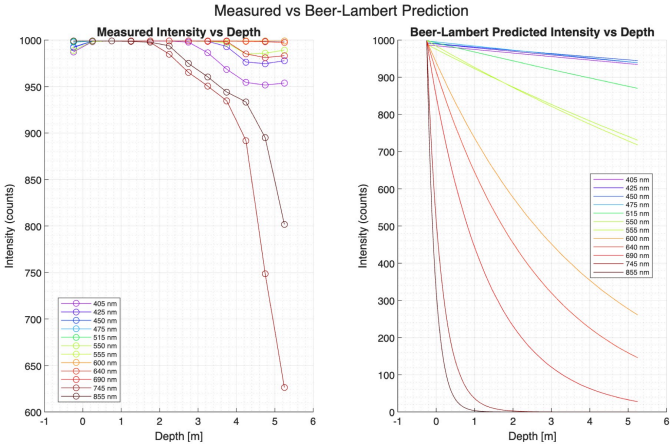

Fig. 14. Data collected by our spectral sensor measuring light intensity across a range of wavelengths against depth alongside a plot of the predicted light intensities by Beer-Lambert [4] using Pope & Fry attenuation constants for pure water [11].

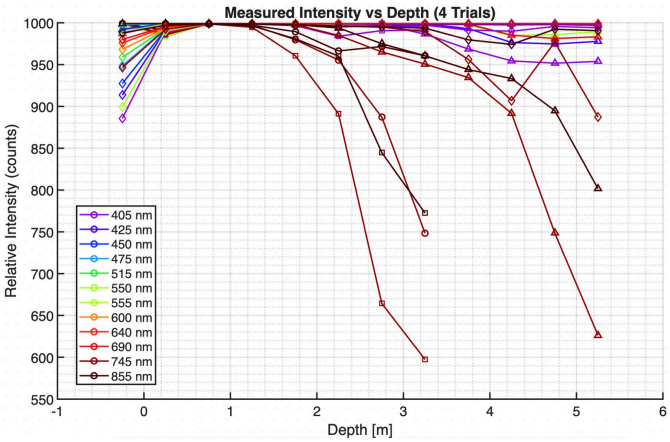

Fig. 15. Plot of measured light intensity over 4 trials at Dana Point.

In Fig. 15 we can see general trends of the 745 nm wavelength attenuated the most, while 855 nm wavelengths are attenuated the second most. The data is a bit unexpected, as applying Beer-Lambert law would give more uniform attenuation. In Fig. 15 we see the data collected is a bit noisy. This data was collected through 2 3-meter dives and 2 5-meter dives. It's strange how the 3 meter dive data shows the 745 nm wavelength attenuated closer to 3 meters, while the 5 meter dive data shows the 745 nm wavelength attenuated closer to 5 meters.

We see the red and orange wavelengths stay the most intense at lower depths compared to other wavelengths. The Beer–Lambert law predicts that light intensity decays exponentially with depth, with attenuation coefficients that depend on wavelength. We would expect shorter wavelengths to penetrate deeper while longer wavelengths are absorbed more rapidly according to Beer-Lambert law [4]. This roughly occurs in Fig. 15, with a possible discrepancy caused by the Dana Point marine environment containing suspended particulates or organic matter that could have favored scattering over simple absorption.

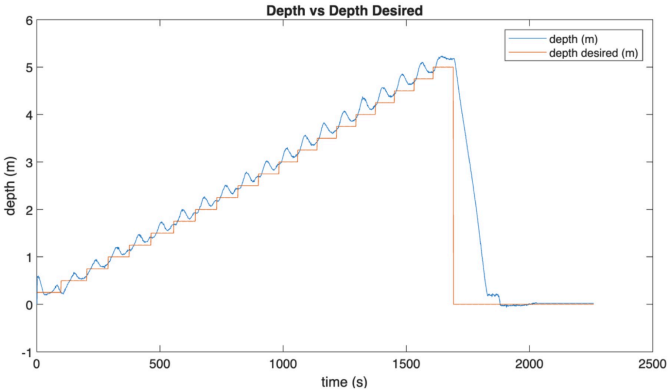

Fig. 16. Plot of robot depth vs depth desired during one of our deployments.

In Fig. 16, we see the robot descending in 0.25 meter increments to over 5 meters deep. A proportional controller is used to calculate how much and which direction the motors should spin. Over the course of the project we adjusted the P constant to make the robot descend at a controlled rate with over dampened characteristics. The drift of the depth from the depth desired accumulates as the robot gets deeper which is interesting. Increasing hydrostatic pressure at greater depths may reduce cavitation effects on the propellers, potentially changing thrust behavior [12]. According to research done on cavitation prediction of ship propeller blades, as water pressure increases with depth, the propeller is less likely to cavitate [12]. This may explain why we saw the amplitude of the overshooting increase as the robot got deeper.

We also had code that would shut off the motors when the robot was within 0.1 meters of the target depth which is partially why there are curves at every increment. The overshooting is likely due to the proportional controller calculating too high of a proportional constant.

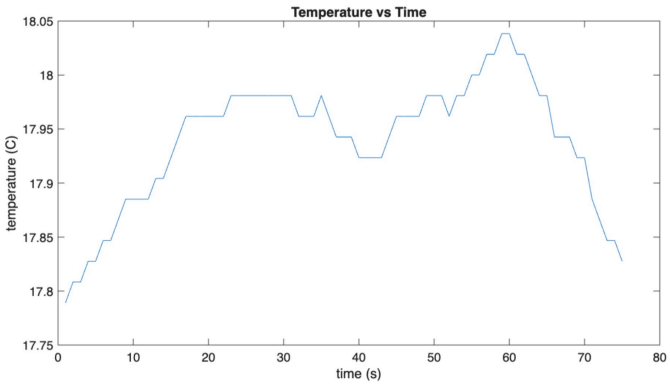

Fig. 17. Temperature vs time plot.

Unfortunately, during our deployments at Dana Point, the thermistor circuit would rail to 0 volts when the robot was fully underwater so we weren't able to collect any data of temperature at different depths. We experienced multiple failed attempts to waterproof the thermistor sensor and learned to waterproof this sensor more carefully in the future. Instead, Fig. 17 shows data of us placing our robot on the surface of the water to get a reading of water temperature from the thermistor. The ground truth water temperature at Dana Point was measured to be 19.5 °C. We see that in Fig. 17, the water temperature roughly 1.5 °C below our ground truth measurement.

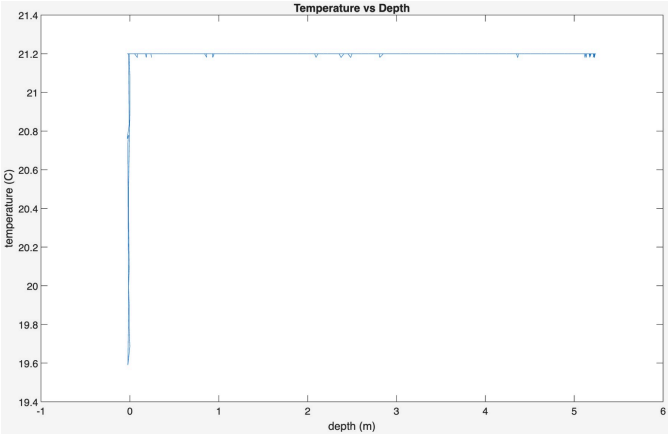

Fig. 18. Plot of thermistor data during a Dana Point trial.

Fig. 18 Shows the thermistor measuring the water temperature to be 19.6 °C at the surface and then railing out to 21.2 °C during the dive. This happened throughout all trials when the thermistor was fully submerged.

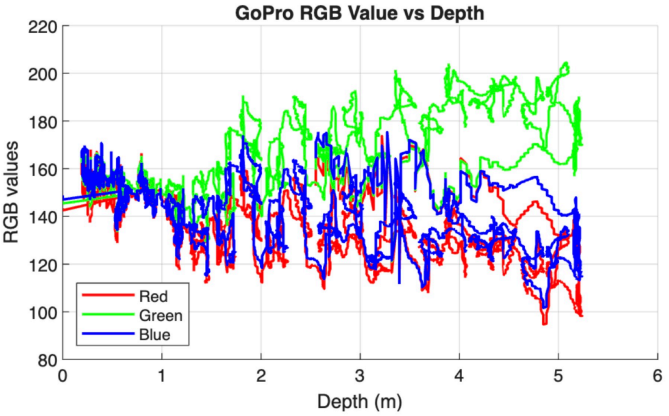

Fig. 19. GoPro RGB values plotted against depth.

In Fig. 19, we see that green light shows up more apparent at higher depths, while red and blue light is attenuated. This does not follow what we expected from Beer-Lambert's law and is likely due to auto-exposure being set to true on the GoPro. This makes the GoPro automatically adjust its exposure level to keep the video bright. As you can see in Fig. 20, the frame shows a mostly green image which is why Fig. 19 shows green light becoming more intense as depth increases.

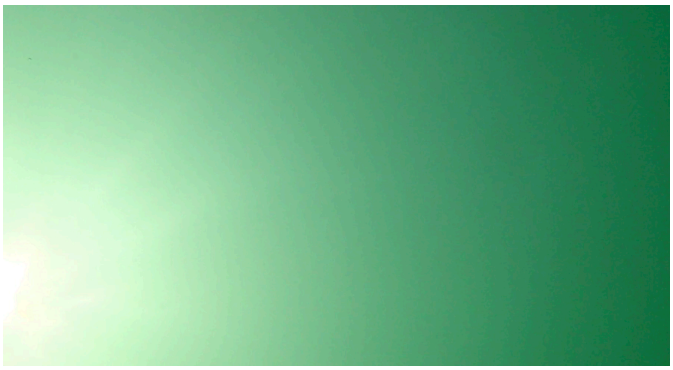

Fig. 20. Frame of video captured by the GoPro during a dive. Sun is visible in the bottom left corner.

VI. Conclusion

The big-picture takeaway is that light does not travel uniformly through water, some wavelengths can travel longer while others get attenuated quicker. We learned that thermistors can change resistance when fully submerged in salt water, and that the 745 nm wavelength of light gets the most attenuated at depths over 3 meters deep. In the future, we need to more carefully waterproof the thermistor sensor, debug why the spectral sensor readings were so noisy, and turn off auto exposure on the GoPro to get more accurate relative intensities. It would also be helpful to have another sensor to measure spectral data, so that we can have more accurate readings. We found that longer wavelengths of light were generally attenuated more than shorter wavelengths which aligns with expectations of the Bouguer-Beer-Lambert law. Experimental data consistently identified the 745 nm wavelength as having the highest attenuation rate at depths exceeding 3 meters.

This work can be used in the future to estimate clarity and composition of water when compared with theoretical and baseline data and to help scientists study water quality and composition. It provides a low cost, foundational framework for using an AUV system to characterize bodies of water and better understand how light behaves in water.

Acknowledgements

I would like to acknowledge Javier, the E80 proctor team (especially Kavi), Prof. Sinopoli, Prof. Lynn, and Prof. Helmns who helped us with this project. The deployments were possible because of the amazing student proctors, staff, and bus drivers that made that day possible. Thank you to Nathan d'Abreu Noronha for peer reviewing my report.

References

[1] J. T. O. Kirk, *Light and photosynthesis in aquatic ecosystems*, 2nd ed. Cambridge: Cambridge University Press, 1994. doi: 10.1017/CBO9780511623370.

[2] O. US EPA, "Indicators: Water Clarity." Accessed: May 08, 2026. [Online]. Available: https://www.epa.gov/national-aquatic-resource-surveys/indicators-water-clarity

[3] N. Girgibo, X. Lü, E. Hiltunen, P. Peura, and Z. Dai, "The air temperature change effect on water quality in the Kvarken Archipelago area," *Science of The Total Environment*, vol. 874, p. 162599, May 2023, doi: 10.1016/j.scitotenv.2023.162599.

[4] T. G. Mayerhöfer, S. Pahlow, and J. Popp, "The Bouguer-Beer-Lambert Law: Shining Light on the Obscure," *ChemPhysChem*, vol. 21, no. 18, pp. 2029–2046, Sep. 2020, doi: 10.1002/cphc.202000464.

[5] "Light and Color in the Deep Sea," *NOAA Ocean Exploration*, Accessed: May 08, 2026. [Online]. Available: https://oceanexplorer.noaa.gov/wp-content/uploads/2025/04/light-and-color-fact-sheet.pdf

[6] ams OSRAM Group, "AS7343 14-Channel Multi-Spectral Sensor." Jun. 07, 2023. Accessed: May 04, 2026. [Online]. Available: https://cdn.sparkfun.com/assets/e/f/3/6/c/AS7343_DS001046_6-00.pdf

[7] "Freescale Semiconductor MPX5700 Data Sheet: Technical Data Rev 10, 10/2012." 2012. Accessed: May 08, 2026. [Online]. Available: https://www.nxp.com/docs/en/data-sheet/MPX5700.pdf

[8] "NXFT15WF104FA1B030." Accessed: May 08, 2026. [Online]. Available: https://www.digikey.com/en/products/detail/murata-electronics/NXFT15WF104FA1B030/3863253

[9] L. A. Moore and C. M. Smith, "Fused silica as an optical material [Invited]," *Optical Materials Express*, vol. 12, no. 8, p. 3043, Aug. 2022, doi: 10.1364/OME.463349.

[10] Gpsnauticalcharts.com, "Fishing & Nautical Charts Web App." Accessed: May 05, 2026. [Online]. Available: https://fishing-app.gpsnauticalcharts.com/i-boating-fishing-web-app/fishing-marine-charts-navigation.html?title=DANA+POINT+HARBOR+boating+app#15.21/33.4574/-117.6837

[11] R. M. Pope and E. S. Fry, "Absorption spectrum (380–700 nm) of pure water II Integrating cavity measurements," *Applied Optics*, vol. 36, no. 33, p. 8710, Nov. 1997, doi: 10.1364/AO.36.008710.

[12] K. Du and Z. Xiong, "Numerical study on the influence of serrated blade edge on propeller cavitation characteristics and efficiency," *AIP Advances*, vol. 15, no. 10, p. 105314, Oct. 2025, doi: 10.1063/5.0286425.